ACS APPLIED NANO MATERIALS
Cite This: ACS Appl. Nano Mater. 2018, 1, 2455−2460
Letter
www.acsanm.org

Synthesis of Two-Dimensional $Nb_{1.33}C$ (MXene) with Randomly Distributed Vacancies by Etching of the Quaternary Solid Solution $(Nb_{2/3}Sc_{1/3})_2AlC$ MAX Phase

J. Halim,[†] J. Palisaitis,[†] J. Lu,[†] J. Thörnberg,[†] E. J. Moon,[‡] M. Precner,[§] P. Eklund,[†] P. O. Å. Persson,[†] M. W. Barsoum,[‡] and J. Rosen*[,†]

[†]Department of Physics, Chemistry, and Biology, Thin Film Physics Division, Linköping University, Linköping, Sweden
[‡]Department of Materials Science and Engineering, Drexel University, Philadelphia, Pennsylvania 19104, United States
[§]Institute of Electrical Engineering, Slovak Academy of Sciences, Bratislava 84104, Slovak Republic

Supporting Information

ABSTRACT: Introducing point defects in two-dimensional (2D) materials can alter or enhance their properties. Here, we demonstrate how etching a laminated $(Nb_{2/3}Sc_{1/3})_2AlC$ MAX phase (solid solution) of both the Sc and Al atoms results in a 2D $Nb_{1.33}C$ material (MXene) with a large number of vacancies and vacancy clusters. This method is applicable to any quaternary, or higher, MAX phase, wherein one of the transition metals is more reactive than the other and could be of vital importance in applications such as catalysis and energy storage. We also report, for the first time, on the existence of solid solution $(Nb_{2/3}Sc_{1/3})_3AlC_2$ and $(Nb_{2/3}Sc_{1/3})_4AlC_3$ phases.

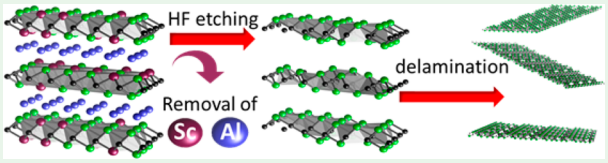

KEYWORDS: *transition-metal carbide, 2D material, synthesis, MXene, electronic properties*

Two-dimensional (2D) materials have shown great promise for many applications.[1−6] The reduced dimension leads to an increase in the surface-to-volume ratio and can fundamentally alter the chemical, optical, and electronic properties of a material. The properties can be altered further, either chemically via surface functionalization[7] and intercalation[8] or structurally by the introduction of defects.[8,9]

About 7 years ago, a new class of 2D materials based on transition-metal carbides and/or nitrides (MXenes) was discovered.[10,11] MXenes are mainly produced by etching the $M_{n+1}AX_n$ (MAX) phases or related ternary phases.[12] The MAX phases are a family of hexagonal, layered ternary transition-metal carbides and/or nitrides where M stands for an early transition metal, A stands mostly for group 13 and 14 elements, X stands for carbon and/or nitrogen, and n = 1, 2, or 3.[13] Various acidic solutions containing fluorine ions are used to selectively etch the A layers (either Al or Ga) and convert MAX to MXene.[10,14−17] The A layers are replaced with oxygen, hydroxyl, and/or fluorine surface-terminating (T) groups.[18] MXenes show promise for a large host of applications including batteries, supercapacitors, transparent conducting electrodes, catalytic and photocatalytic applications, water treatment, electromagnetic shielding, gas sensors, and biosensors.[19−25]

MXene properties can be tuned in at least three ways, which involve altering their (i) composition, (ii) surface terminations, T_x, and/or, (iii) structure/morphology. The composition can be changed by, e.g., forming solid solutions, though alloying on the M,[26] and/or X[27] sites in the parent MAX phase. The quaternaries $(Nb_{0.8},Ti_{0.2})_4C_3T_x$ and $(Nb_{0.8},Zr_{0.2})_4C_3T_x$[28] are examples in which M-site MAX solid-solution phases were etched to produce their MXenes. Ti_3CNT_x is an example of a MXene with an X-site solid solution.[11] Altering the surface terminations can be accomplished by chemical treatment such as alkali treatment and/or postetching heat treatment to remove fluorine terminations.[29,30]

Quite recently, quaternary n = 1, or 211, MAX phases with in-plane chemical ordering were discovered. These phases were labeled *i*-MAX because of the ordering of two different M elements, in a 2:1 ratio, in the basal planes. The first example was $(Mo_{2/3}Sc_{1/3})_2AlC$.[31] When this phase was etched, both the Al and Sc atoms were removed and a MXene—$Mo_{1.33}CTx$ wherein the vacancies were ordered—was produced. This vacancy-ordered 2D material exhibited a 3 orders of magnitude higher electrical conductivity and a 65% higher capacitance when used as a supercapacitor electrode compared to Mo_2CT_x. Furthermore, an ultrathin flexible $Mo_{1.33}CT_x$/polymer film showed promising performance as a solid-state supercapacitor.[32] Since then, other *i*-MAX phases have been theoretically predicted and synthesized such as $(V_{2/3}Zr_{1/3})_2AlC$, $(Mo_{2/3}Y_{1/3})_2AlC$, and $(Cr_{2/3}Sc_{1/3})_2AlC$.[33,34] A characteristic feature of the *i*-MAX phase is that the minority M elements extend from the M toward the Al layers, with a structure described by $C2/c$ or $C2/m$ symmetry.[32] This is opposed to the traditional MAX phase of $P6_3/mmc$ symmetry, which describes most of the solid solution quaternary 211 MAX phases realized.

Received: February 28, 2018
Accepted: April 13, 2018
Published: May 30, 2018

DOI: 10.1021/acsanm.8b00332
ACS Appl. Nano Mater. 2018, 1, 2455−2460

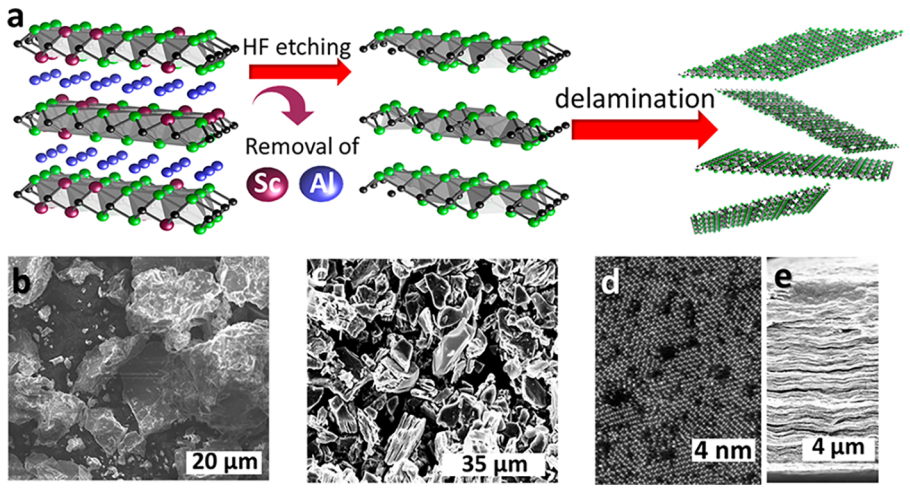

Figure 1. (a) Schematic of the synthesis, etching, and delamination of $(Nb_{2/3}Sc_{1/3})_2AlC$ to form $Nb_{1.33}CT_x$. Green, black, red, and blue represent Nb, C, Sc, and Al atoms, respectively. (b) SEM micrograph of $(Nb_{2/3}Sc_{1/3})_2AlC$ powders. (c) SEM micrograph of multilayered $Nb_{1.33}CT_x$ powders. (d) STEM micrograph of a single $Nb_{1.33}CT_x$ flake, (e) SEM micrograph of the cross section of a free-standing film made from d-$Nb_{1.33}CT_x$.

A large majority of MXene work to date has been carried out on $Ti_3C_2T_x$. There are others, however. Recently, Nb_2CT_x flakes have shown promising performance for photothermal cell ablation and as a photocatalyst for hydrogen evolution in addition to previously reported results for energy storage applications.[35−38] These reports were the impetus for this work, together with our recent discovery of a quaternary *i*-MAX phase in which the minority M element, Sc in this case, was readily etched.

First, we synthesized the new quaternary MAX solid solution, $(Nb_{2/3}Sc_{1/3})_2AlC$, wherein the M elements Nb and Sc are not ordered. We then selectively etched both Al and Sc atoms to produce $Nb_{1.33}CT_x$, with randomly distributed vacancies and vacancy clusters. A schematic of our approach is shown in Figure 1a. In principle, this method should be applicable to any quaternary MAX phase in which the minority M element is etchable.

The quaternary solid solution $(Nb_{2/3}Sc_{1/3})_2AlC$ was synthesized by reacting the elemental powders Nb, Sc, Al, and, C in a molar ratio of $^4/_3$:$^2/_3$:1:1 at 1400 °C for 2 h in flowing Ar (processing details can be found in the Supporting Information). The crystal structure is shown in the leftmost panel in Figure 1a. Parts b and c of Figure 1 show scanning electron microscopy (SEM) images of the $(Nb_{2/3}Sc_{1/3})_2AlC$ powders before and after etching, respectively. Figure 1d shows a typical scanning transmission electron microscopy (STEM) image of a single $Nb_{1.33}CT_x$ flake showing vacancies and vacancy clusters. The removal of Sc atoms was confirmed by electron energy loss spectroscopy analysis (see Figure S1). Figure 1e shows a cross-sectional SEM image of a free-standing thin film made by filtering delaminated (d-)$Nb_{1.33}CT_x$ flakes.

The STEM images, shown in Figure 2a,b, show the typical MAX-phase-layered structure.[13] The MAX-phase identification is further confirmed by selected-area electron diffraction (SAED; Figure 2a,b, insets). Rietveld refinement analysis of a powder X-ray diffraction (XRD) pattern (Figure 2c) was used to quantify the various phases present. According to Rietveld analysis (refinement details can be found in the Supporting Information), the sample contained the following phases: $(Nb_{2/3}Sc_{1/3})_2AlC$, $NbAl_3$, NbC, $(Nb_{2/3}Sc_{1/3})_3AlC_2$, and $(Nb_{2/3}Sc_{1/3})_4AlC_3$ with weight percentages of 68(2), 10.1(4), 17.4(4), 2.5(3), and 2.0(2) wt %, respectively. When all of the

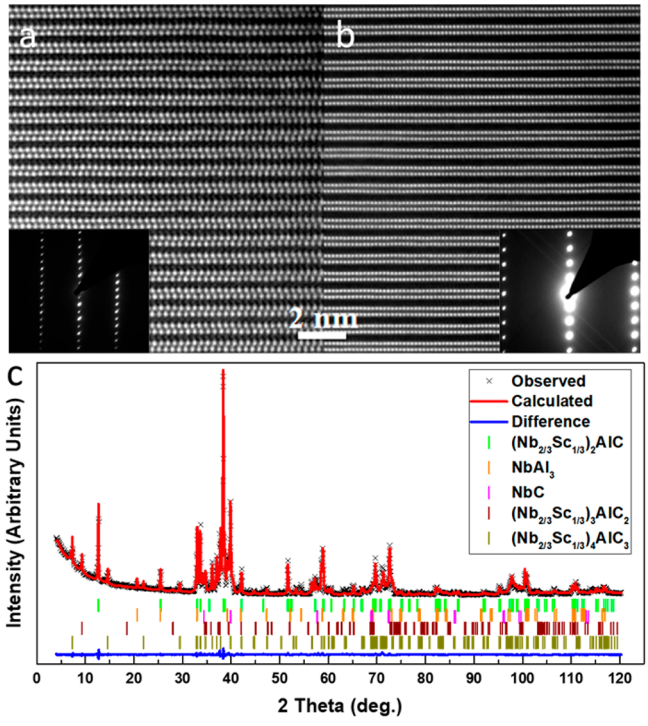

Figure 2. (a) STEM micrograph with SAED of $(Nb_{2/3}Sc_{1/3})_2AlC$ in the $[11\bar{2}0]$ zone axis. (b) Same as part a but in the $[10\bar{1}0]$ zone axes. (c) XRD patterns indexed to a $(Nb_{2/3}Sc_{1/3})_2AlC$ powder showing the observed pattern (black crosses), the Rietveld-generated pattern (red line), and the difference between the two (blue line). The green, orange, purple, violet, and olive ticks below the pattern represent the peak positions of $(Nb_{2/3}Sc_{1/3})_2AlC$, $NbAl_3$, NbC, $(Nb_{2/3}Sc_{1/3})_3AlC_2$, and $(Nb_{2/3}Sc_{1/3})_4AlC_3$ phases, respectively.

phases were considered, the χ^2 value was 8.78. Note that the powder showed evidence for $(Nb_{2/3}Sc_{1/3})_{n+1}AlC_n$, with n = 1−3.

For the main phase $(Nb_{2/3}Sc_{1/3})_2AlC$, because Nb and Sc are randomly distributed in the transition-metal position, the quaternary MAX phase retains the $P6_3/mmc$ symmetry of the ternary MAX phases. The a and c lattice parameters were calculated to be 3.12915(5) and 13.9736(3) Å, respectively, which agree with those obtained from STEM and SAED. These

DOI: 10.1021/acsanm.8b00332
ACS Appl. Nano Mater. 2018, 1, 2455−2460

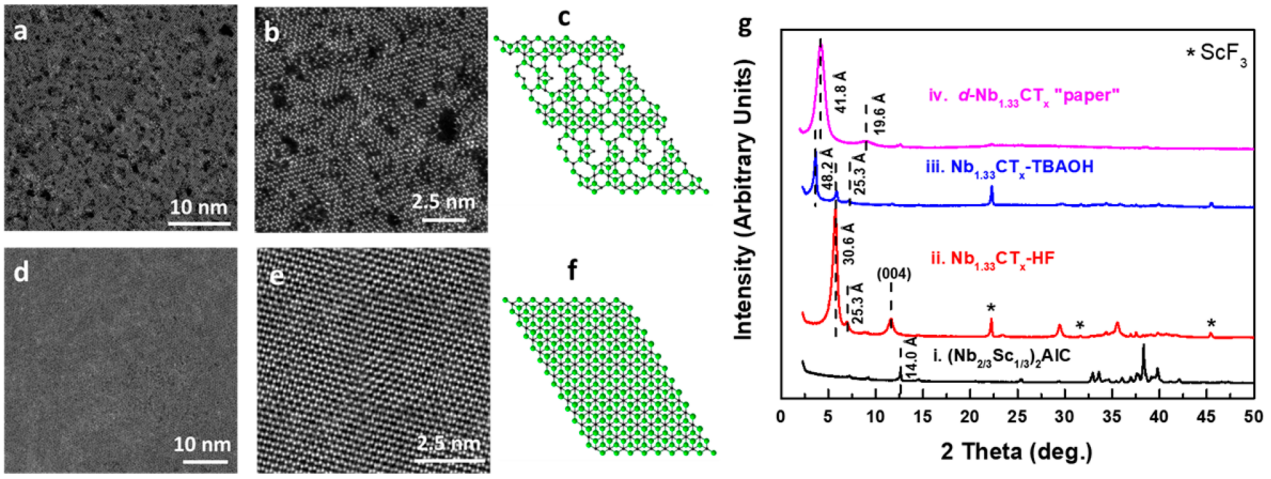

Figure 3. (a) Low-magnification STEM micrograph of a $Nb_{1.33}CT_x$ single flake. (b) Same as panel (a) but at higher magnification. (c) Top-view schematic of a single $Nb_{1.33}CT_x$ sheet showing random vacancies and vacancy clusters. (d) Low-magnification STEM micrograph of a Nb_2CT_x single flake. (e) Same as panel (d) but at higher magnification. (f) Top-view schematic of a single Nb_2CT_x sheet. (g) XRD patterns of (i) $(Nb_{2/3}Sc_{1/3})_2AlC$, (ii) $Nb_{1.33}CT_x$–HF, which is that of MLs after HF etching of $(Nb_{2/3}Sc_{1/3})_2AlC$ powders, (iii) $Nb_{1.33}CT_x$–HF–TBAOH, which is $Nb_{1.33}CT_x$ after intercalation with TBAOH, and (iv) a d-$Nb_{1.33}CT_x$ film obtained by filtering a suspension of d-$Nb_{1.33}CT_x$ (Figure 1e). Peaks denoted by asterisks correspond to ScF_3, which is a residue of etching.

lattice parameters are slightly larger than those of Nb_2AlC (a = 3.096–3.126 Å and c = 13.804–13.888 Å).[39] The difference can be ascribed to the larger metallic radius of Sc (160 pm) compared to Nb (145 pm).[40] Similarly, and likely for the same reason, the lattice parameters of $(Nb_{2/3}Sc_{1/3})_4AlC_3$ [a = 3.1855(5) Å and c = 23.878(6) Å] are slightly larger than those of Nb_4AlC_3 (a = 3.1296 Å and c = 24.1208 Å).[41] Despite the fact that to date Nb_3AlC_2 has not been experimentally realized, the introduction of Sc appears to stabilize the $(Nb_{2/3}Sc_{1/3})_3AlC_2$ solid solution. This has also been reported for other 312 phases, where a second M element stabilizes an otherwise unstable 312 phase.[42,43]

According to energy-dispersive X-ray spectroscopy (EDS) of individual MAX-phase particles assumed to be $(Nb_{2/3}Sc_{1/3})_2AlC$, the Nb:Sc:Al atomic ratio was 1.2:0.8:1.0 (details of EDS analysis can be found in the Supporting Information). From the Rietveld refinment of the Nb and Sc occupancies in the same phase, the Nb:Sc atomic ratio was found to be 1.38:0.62. It is thus reasonable to conclude that the Nb:Sc ratio is between 1.2:0.8 and 1.4:0.6. At 2:1.33 to 2:0.86, respectively, these ratios bracket the nominal ratio of 2:1.

The MXene synthesis details can be found in the Supporting Information. Immersing $(Nb_{2/3}Sc_{1/3})_2AlC$ powders in 48% concentrated hydrofluoric acid (HF) at room temperature for 30 h resulted in selective etching of the majority of both of the Al and Sc atoms, creating $Nb_{1.33}CT_x$ multilayers (MLs; Figure 1c). Clearly, the Sc atoms are more reactive than the Nb atoms, which is consistent with theoretical calculations, which have shown that the Sc–C and C–Al bonds in Sc_2AlC are of comparable strength and both weaker than the Nb–C or Nb–Al bonds in Nb_2AlC.[44]

To obtain $Nb_{1.33}CT_x$ monolayers, the ML powder was intercalated with tetrabutylammonium hydroxide (TBAOH) in water following the procedure described by Naguib et al.,[45] followed by delamination in water by hand shaking, yielding a ≈1 mg/mL suspension of, most probably, single MXene flakes in water. To produce a d-Nb_2CT_x suspension starting with Nb_2AlC, using the same method, the etching time had to be increased to 100 h—compared to 30 h for $(Nb_{2/3}Sc_{1/3})_2AlC$—yielding a colloidal suspension with a concentration of <0.5 mg/mL. Hence, the introduction of Sc in the MAX phase improves the yield and reduces the etching time.

Upon filtering of the $Nb_{1.33}CT_x$ and Nb_2CT_x suspensions, only the former formed flexible, free-standing films that were easy to handle. The latter formed a brittle film that could not be peeled off of the filter membrane without breaking into small pieces. It is for this reason that no transport properties are reported for this compound.

A typical morphology of a $Nb_{1.33}CT_x$ single flake can be seen in the STEM images in Figure 3a,b and can be compared to the schematic shown in Figure 3c. The flakes contain vacancies and vacancy clusters ranging in size between 0.1 and 2 nm, resulting from removal of the Sc atoms. The vacancies' areal coverage varied from 20% to 35% depending on the area imaged (see Figure S2). STEM images of Nb_2CT_x single flakes, on the other hand, are shown in Figure 3d,e. In this case, the MXene layers, shown schematically in Figure 3f, are quite visibly less defective. The XRD patterns of the etched material (Figure 3g) show the typical increase in the interlayer spacing, denoted as $d_{c/2}$ [because it is $^1/_2$ the c-LP of the (002) parent MAX], to that of the parent phase [compare parts g(i) and g(ii) of Figure 3]. This is typical of the MAX-to-MXene conversion and reflects the substitution of Al with surface terminations of –O, –OH, and/or –F and multiple water layers.[45,46] No residual peaks of the parent phase are present after etching, indicating a complete MAX-to-MXene conversion. However, peaks corresponding to ScF_3, denoted by asterisks, were present. After TBAOH intercalation, $d_{c/2}$ increases to 24.1 Å [Figure 3g(iii)], reflecting intercalation of the TBA^+ ions and more water molecules. After filtering of the suspension to form a free-standing film [Figure 3g(iv)], $d_{c/2}$ is reduced to 20.9 Å presumably because of the removal of some of the water molecules and possibly TBA^+ ions.

High-resolution X-ray photoelectron spectroscopy (XPS) spectra, with peak fits of a d-$Nb_{1.33}CT_x$ filtered film, are shown in parts a–d of Figure 4 for the Nb 3d, C 1s, O 1s, and F 1s regions, respectively. The peak-fitting results and elemental compositions extracted from the high-resolution spectra can be

DOI: 10.1021/acsanm.8b00332
ACS Appl. Nano Mater. 2018, 1, 2455–2460

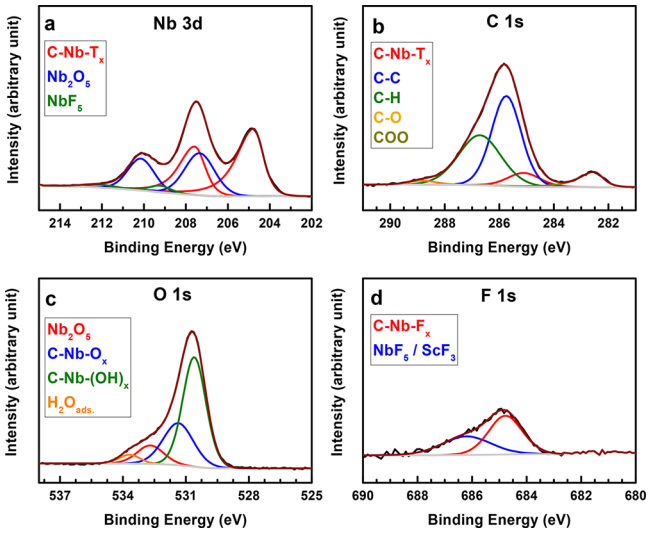

Figure 4. XPS spectra of the d-$Nb_{1.33}CT_x$ film for the (a) Nb 3d, (b) C 1s, (c) O 1s, and (d) F 1s regions. Color-coded fitting peaks represent various assigned species (Table S4).

found in the Supporting Information. On the basis of the extracted atomic percentages of Nb, C, O, and F and the fraction of each species solely related to the 2D flakes, the chemical formula that best describes d-$Nb_{1.33}CT_x$ is $Nb_{1.33}CO_{1.7}(OH)_{0.6}F_{0.2}{\cdot}0.2H_2O$, while that for d-$Nb_2CT_x$ is $Nb_2CO(OH)_{0.6}F_{0.1}{\cdot}0.3H_2O{\cdot}0.3N$. (The C peak associated with MXene was used as the reference with a base error of <±0.1.) The XPS results for d-Nb_2CT_x can be found in the Supporting Information. The N component originates from the intercalated TBAOH, a component that was not possible to extract from the d-$Nb_{1.33}CT_x$ flakes because of the overlap between the N 1s and Sc 2p peaks (Figure S3b). It is clear that −O is the dominant termination for both compounds. Interestingly, it is >1.5 times higher in d-$Nb_{1.33}CT_x$ compared to d-Nb_2CT_x. The amounts of −OH and −F are comparable in both samples. Note that the fraction of −F surface terminations for both compounds is low, which is common for MXenes treated with TBAOH.[45,46] At 2.5, the total number of termination moles for d-$Nb_{1.33}CT_x$ is 0.5 higher than the theoretical value of 2 obtained when all surface sites are filled.[47] This suggests that some of the surface terminations may very well reside in the vacancies that result from the removal of Sc atoms and are thus, strictly speaking, no longer terminations. The total moles of terminations for d-Nb_2CT_x, excluding N, is 1.7, which is less than 2.

A semilog plot of the resistivity, ρ, versus temperature, T, of a 22-μm-thick d-$Nb_{1.33}CT_x$ film is shown in Figure 5a. The details of the measurements can be found in the Supporting Information. As the temperature decreases from 300 to 7 K, ρ increases from 556 to 1.5 x 10^6 mΩ·m. To shed more light on the transport mechanism, the ρ data in the 7−300 K temperature range were fitted to several models, including 2D, 3D, and Efros−Shklovskii (E−S), variable range hopping (VRH), simple thermal activation, and power-law (nonexponential) models. The fitting results (Figures 5b and S5) clearly eliminate the latter two (Figure S5). The same results, however, cannot differentiate between the various VRH models; the R^2 values for the 2D, E−S, and 3D VRH models are comparable, 0.9980, 0.9978, and 0.9964, respectively. Figure 5b plots the results for the most likely model, viz., 2D VRH; the other fits for the other models can be found in Figure S5. Similar behavior has been reported for the other MXene films such as Mo_2CT_x,[46] $Mo_2TiC_2T_x$, and $Mo_2Ti_2C_3T_x$.[48]

Magnetoresistance (MR) measurements, performed at 10 K, showed negative MR, which is in contradistinction with the MR measurements on other MXene compounds exhibiting the VRH mechanism.[46,48] However, other disordered materials showing VRH, such as In_2O_{3-x}, and Si doped in GaAs have been reported to exhibit negative MR.[49−51] The negative MR for materials having VRH conduction mechanisms has been ascribed to several reasons such as quantum interference, the Zeeman effect, or localized magnetic moments.[52] These comments notwithstanding, much more work, which is beyond the scope of this paper, is needed to obtain a deeper understanding of conduction in our films.

In conclusion, a facile, reproducible, relatively rapid method for producing random vacancies and vacancy clusters in MXenes is presented, where the minority M element in a quaternary solid-solution MAX phase is concomitantly etched with the A-group element. Herein we synthesized $(Nb_{2/3}Sc_{1/3})_2AlC$ and selectively etched both the Sc and Al atoms to produce $Nb_{1.33}CT_x$ with disordered vacancies. The presence of Sc in the quaternary MAX phase decreased the

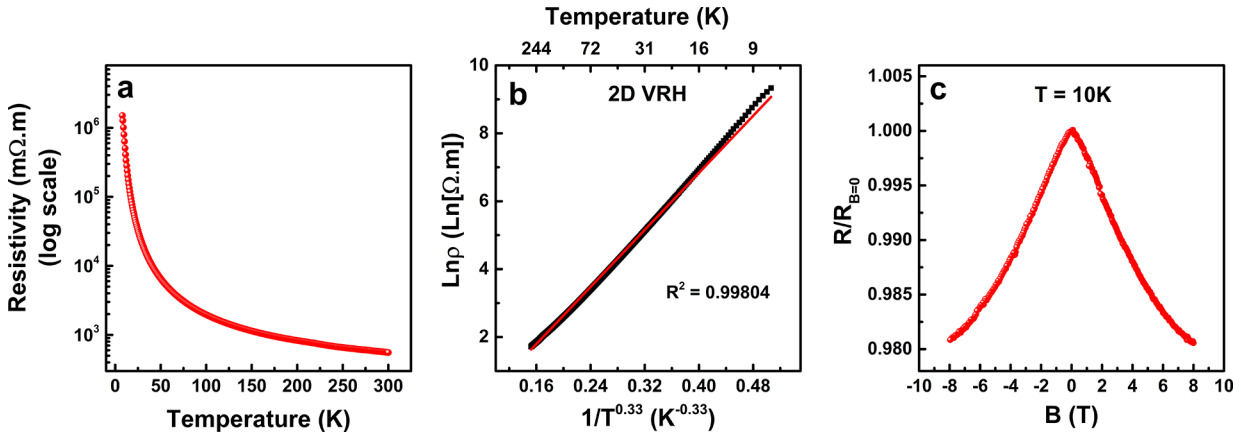

Figure 5. Electronic transport characteristics of the d-$Nb_{1.33}CT_x$ film on temperature and magnetic field: (a) Log of resistivity, ρ, versus temperature in the 7−300 K temperature range, (b) ρ versus $1/T^{1/3}$ in the 7−300 K temperature range assuming 2D VRH conduction model, and (c) MR at 10 K. $R_{B=0}$ refers to resistance in the absence of a magnetic field.

DOI: 10.1021/acsanm.8b00332
ACS Appl. Nano Mater. 2018, 1, 2455−2460

etching time from 100 to 30 h and increased the yield of delaminated flakes.

When $Nb_{1.33}CT_x$ free-standing films were cooled from 300 to 7 K, their resistivity increased from 556 to 1.5 x 10^6 mΩ·m. The suggested transport mechanism is VRH accompanied by negative MR at 10 K. Last, there is no reason that this approach cannot be used to "dial-in" a controlled number of vacancies, as long as the parent solid-solution MAX phase exists. The fact that the flakes with vacancies are less dense than their counterparts is also noteworthy when specific properties are sought.

■ ASSOCIATED CONTENT

Supporting Information

The Supporting Information is available free of charge on the ACS Publications website at DOI: 10.1021/acsanm.8b00332.

Synthesis of materials, characterization techniques, Rietveld refinement, EDS, electron energy loss spectra, statistical image analysis, XPS spectra, and transport analysis (PDF)

■ AUTHOR INFORMATION

Corresponding Author

*E-mail: johanna.rosen@liu.se.

ORCID

J. Halim: 0000-0002-7502-1215

P. Eklund: 0000-0003-1785-0864

J. Rosen: 0000-0002-5173-6726

Author Contributions

J.H. synthesized the material and performed the XRD, XPS characterization, and analysis. M.P. performed the transport measurements. M.P., E.J.M., and J.H. analyzed the transport data. J.T. performed the SEM and EDX characterization and analyzed the data. J.P. and J.L. performed the STEM characterization and analyzed the data. P.P., M.W.B., and J.R. supervised the research. All authors contributed to the preparation of the manuscript and in discussions. All authors have given approval to the final version of the manuscript.

Notes

The authors declare no competing financial interest.

■ ACKNOWLEDGMENTS

We acknowledge support from the Swedish Foundation for Strategic Research through the Synergy Grant FUNCASE and Research Infrastructure Fellowship RIF 14-0074 and from the Knut and Alice Wallenberg (KAW) Foundation for Fellowship Grants, Project funding (KAW 2015.0043), and support toward the Linköping Electron Microscopy Laboratory. The Swedish Research Council is gratefully acknowledged for Projects 642-2013-8020 and 621-2014-4890. We also acknowledge the Swedish Government Strategic Research Area in Materials Science on Functional Materials at Linköping University (Faculty Grant SFO-Mat-LiU No. 2009-00971).

■ REFERENCES

(1) Mas-Balleste, R.; Gomez-Navarro, C.; Gomez-Herrero, J.; Zamora, F. 2D Materials: to Graphene and Beyond. *Nanoscale* **2011**, *3*, 20−30.

(2) Fiori, G.; Bonaccorso, F.; Iannaccone, G.; Palacios, T.; Neumaier, D.; Seabaugh, A.; Banerjee, S. K.; Colombo, L. Electronics Based on Two-Dimensional Materials. *Nat. Nanotechnol.* **2014**, *9*, 768−779.

(3) Sup Choi, M.; Lee, G.-H.; Yu, Y.-J.; Lee, D.-Y.; Hwan Lee, S.; Kim, P.; Hone, J.; Jong Yoo, W. Controlled Charge Trapping by Molybdenum Disulphide and Graphene in Ultrathin Heterostructured Memory Devices. *Nat. Commun.* **2013**, *4*, 1624.

(4) Bernardi, M.; Palummo, M.; Grossman, J. C. Extraordinary Sunlight Absorption and One Nanometer Thick Photovoltaics Using Two-Dimensional Monolayer Materials. *Nano Lett.* **2013**, *13*, 3664−3670.

(5) Surwade, S. P.; Smirnov, S. N.; Vlassiouk, I. V.; Unocic, R. R.; Veith, G. M.; Dai, S.; Mahurin, S. M. Water Desalination Using Nanoporous Single-Layer Graphene. *Nat. Nanotechnol.* **2015**, *10*, 459−464.

(6) Bonaccorso, F.; Colombo, L.; Yu, G.; Stoller, M.; Tozzini, V.; Ferrari, A. C.; Ruoff, R. S.; Pellegrini, V. Graphene, Related Two-Dimensional Crystals, and Hybrid Systems for Energy Conversion and Storage. *Science* **2015**, *347*, 1246501.

(7) Liu, Z.; Lau, S. P.; Yan, F. Functionalized Graphene and Other Two-Dimensional Materials for Photovoltaic Devices: Device Design and Processing. *Chem. Soc. Rev.* **2015**, *44*, 5638−5679.

(8) Wan, J.; Lacey, S. D.; Dai, J.; Bao, W.; Fuhrer, M. S.; Hu, L. Tuning Two-Dimensional Nanomaterials by Intercalation: Materials, Properties and Applications. *Chem. Soc. Rev.* **2016**, *45*, 6742−6765.

(9) Amani, M.; Lien, D.-H.; Kiriya, D.; Xiao, J.; Azcatl, A.; Noh, J.; Madhvapathy, S. R.; Addou, R.; Santosh, K.; Dubey, M.; et al. Near-unity Photoluminescence Quantum Yield in MoS_2. *Science* **2015**, *350*, 1065−1068.

(10) Naguib, M.; Kurtoglu, M.; Presser, V.; Lu, J.; Niu, J. J.; Heon, M.; Hultman, L.; Gogotsi, Y.; Barsoum, M. W. Two-Dimensional Nanocrystals Produced by Exfoliation of Ti_3AlC_2. *Adv. Mater.* **2011**, *23*, 4248−4253.

(11) Naguib, M.; Mashtalir, O.; Carle, J.; Presser, V.; Lu, J.; Hultman, L.; Gogotsi, Y.; Barsoum, M. W. Two-Dimensional Transition Metal Carbides. *ACS Nano* **2012**, *6*, 1322−31.

(12) Zhou, J.; Zha, X.; Chen, F. Y.; Ye, Q.; Eklund, P.; Du, S.; Huang, Q. A Two-Dimensional Zirconium Carbide by Selective Etching of Al_3C_3 from Nanolaminated $Zr_3Al_3C_5$. *Angew. Chem., Int. Ed.* **2016**, *55*, 5008−5013.

(13) Barsoum, M. W. *MAX Phases: Properties of Machinable Ternary Carbides and Nitrides*; John Wiley & Sons, 2013.

(14) Halim, J.; Lukatskaya, M. R.; Cook, K. M.; Lu, J.; Smith, C. R.; Näslund, L.-Å.; May, S. J.; Hultman, L.; Gogotsi, Y.; Eklund, P.; Barsoum, M. W. Transparent Conductive Two-Dimensional Titanium Carbide Epitaxial Thin Films. *Chem. Mater.* **2014**, *26*, 2374−2381.

(15) Ghidiu, M.; Lukatskaya, M. R.; Zhao, M.-Q.; Gogotsi, Y.; Barsoum, M. W. Conductive Two-Dimensional Titanium Carbide 'Clay' with High Volumetric Capacitance. *Nature* **2014**, *516*, 78−81.

(16) Ghidiu, M.; Halim, J.; Kota, S.; Bish, D.; Gogotsi, Y.; Barsoum, M. W. Ion-Exchange and Cation Solvation Reactions in Ti_3C_2 MXene. *Chem. Mater.* **2016**, *28*, 3507−3514.

(17) Liu, F.; Zhou, J.; Wang, S.; Wang, B.; Shen, C.; Wang, L.; Hu, Q.; Huang, Q.; Zhou, A. Preparation of High-Purity V_2C MXene and Electrochemical Properties as Li-Ion Batteries. *J. Electrochem. Soc.* **2017**, *164*, A709−A713.

(18) Halim, J.; Cook, K. M.; Naguib, M.; Eklund, P.; Gogotsi, Y.; Rosen, J.; Barsoum, M. W. X-Ray Photoelectron Spectroscopy of Select Multi-layered Transition Metal Carbides (MXenes). *Appl. Surf. Sci.* **2016**, *362*, 406−417.

(19) Hong Ng, V. M.; Huang, H.; Zhou, K.; Lee, P. S.; Que, W.; Xu, J. Z.; Kong, L. B. Recent Progress in Layered Transition Metal Carbides and/or Nitrides (MXenes) and their Composites: Synthesis and Applications. *J. Mater. Chem. A* **2017**, *5*, 3039−3068.

(20) Lukatskaya, M. R.; Kota, S.; Lin, Z.; Zhao, M.-Q.; Shpigel, N.; Levi, M. D.; Halim, J.; Taberna, P.-L.; Barsoum, M. W.; Simon, P.; Gogotsi, Y. Ultra-high-rate Pseudocapacitive Energy Storage in Two-Dimensional Transition Metal Carbides. *Nature Energy* **2017**, *2*, 17105.

(21) Ying, G.; Kota, S.; Dillon, A. D.; Fafarman, A. T.; Barsoum, M. Conductive Transparent V_2T_x(MXene) Films. *FlatChem* **2018**, *8*, 25−30.

DOI: 10.1021/acsanm.8b00332
ACS Appl. Nano Mater. 2018, 1, 2455−2460

(22) Naguib, M.; Mochalin, V. N.; Barsoum, M. W.; Gogotsi, Y. 25th Anniversary Article: MXenes: A New Family of Two-Dimensional Materials. *Adv. Mater.* **2014**, *26*, 992−1005.
(23) Anasori, B.; Lukatskaya, M. R.; Gogotsi, Y. 2D Metal Carbides and Nitrides (MXenes) for Energy Storage. *Nature Reviews Materials* **2017**, *2*, 16098.
(24) Eklund, P.; Rosen, J.; Persson, P. O. Å. Layered Ternary $M_{n+1}AX_n$ Phases and their 2D Derivative MXene: An Overview from a Thin-film Perspective. *J. Phys. D: Appl. Phys.* **2017**, *50*, 113001.
(25) Sun, S.; Liao, C.; Hafez, A. M.; Zhu, H.; Wu, S. Two-Dimensional MXenes for Energy Storage. *Chem. Eng. J. (Amsterdam, Neth.)* **2018**, *338*, 27−45.
(26) Naguib, M.; Bentzel, G. W.; Shah, J.; Halim, J.; Caspi, E. N.; Lu, J.; Hultman, L.; Barsoum, M. W. New Solid Solution MAX Phases: $(Ti_{0.5},V_{0.5})_3AlC_2$, $(Nb_{0.5},V_{0.5})_2AlC$, $(Nb_{0.5},V_{0.5})_4AlC_3$ and $(Nb_{0.8},Zr_{0.2})_2AlC$. *Mater. Res. Lett.* **2014**, *2*, 233−240.
(27) Manoun, B.; Saxena, S.; Hug, G.; Ganguly, A.; Hoffman, E.; Barsoum, M. Synthesis and Compressibility of $Ti_3(Al,Sn_{0.2})C_2$ and $Ti_3Al(C_{0.5},N_{0.5})_2$. *J. Appl. Phys.* **2007**, *101*, 113523.
(28) Yang, J.; Naguib, M.; Ghidiu, M.; Pan, L.-M.; Gu, J.; Nanda, J.; Halim, J.; Gogotsi, Y.; Barsoum, M. W. Two-Dimensional Nb-Based M_4C_3 Solid Solutions (MXenes). *J. Am. Ceram. Soc.* **2016**, *99*, 660−666.
(29) Dall'Agnese, Y.; Lukatskaya, M. R.; Cook, K. M.; Taberna, P.-L.; Gogotsi, Y.; Simon, P. High Capacitance of Surface-modified 2D Titanium Carbide in Acidic Electrolyte. *Electrochem. Commun.* **2014**, *48*, 118−122.
(30) Persson, I.; Näslund, L.-Å.; Halim, J.; Barsoum, M. W.; Darakchieva, V.; Palisaitis, J.; Rosen, J.; Persson, P. O. Å. On the Organization and Thermal Behavior of Functional Groups on Ti_3C_2 MXene Surfaces in Vacuum. *2D Mater.* **2018**, *5*, 015002.
(31) Tao, Q.; Dahlqvist, M.; Lu, J.; Kota, S.; Meshkian, R.; Halim, J.; Palisaitis, J.; Hultman, L.; Barsoum, M. W.; Persson, P. O.; Rosen, J. Two-dimensional $Mo_{1.33}C$ MXene with Divacancy Ordering Prepared from Parent 3D Laminate with In-plane Chemical Ordering. *Nat. Commun.* **2017**, *8*, 14949.
(32) Qin, L.; Tao, Q.; El Ghazaly, A.; Fernandez-Rodriguez, J.; Persson, P. O. Å.; Rosen, J.; Zhang, F. High-Performance Ultrathin Flexible Solid-State Supercapacitors Based on Solution Processable $Mo_{1.33}C$ MXene abd PEDOT:PSS. *Adv. Funct. Mater.* **2018**, *28*, 1703808.
(33) Dahlqvist, M.; Lu, J.; Meshkian, R.; Tao, Q.; Hultman, L.; Rosen, J. Prediction and Synthesis of a Family of Atomic Laminate Phases with Kagomé-like and In-plane Chemical Ordering. *Science Advances* **2017**, *3*, e1700642.
(34) Lu, J.; Thore, A.; Meshkian, R.; Tao, Q.; Hultman, L.; Rosen, J. Theoretical and Experimental Exploration of a Novel In-plane Chemically-ordered $(Cr_{2/3}M_{1/3})_2AlC$ i-MAX Phase with M= Sc and Y. *Cryst. Growth Des.* **2017**, *17*, 5704−5711.
(35) Lin, H.; Gao, S.; Dai, C.; Chen, Y.; Shi, J. Two-Dimensional Biodegradable Niobium Carbide (MXene) for Photothermal Tumor Eradication in NIR-I and NIR-II Bio-Windows. *J. Am. Chem. Soc.* **2017**, *139*, 16235−16247.
(36) Mashtalir, O.; Lukatskaya, M. R.; Zhao, M. Q.; Barsoum, M. W.; Gogotsi, Y. Amine-assisted Delamination of Nb_2C MXene for Li-Ion Energy Storage Devices. *Adv. Mater.* **2015**, *27*, 3501−3506.
(37) Naguib, M.; Halim, J.; Lu, J.; Cook, K. M.; Hultman, L.; Gogotsi, Y.; Barsoum, M. W. New Two-dimensional Niobium and Vanadium Carbides as Promising Materials for Li-ion Batteries. *J. Am. Chem. Soc.* **2013**, *135*, 15966−9.
(38) Su, T.; Peng, R.; Hood, Z. D.; Naguib, M.; Ivanov, I. N.; Keum, J. K.; Qin, Z.; Guo, Z.; Wu, Z. One-step Synthesis of $Nb_2O_5/C/Nb_2C$ (MXene) Composites and their Use as Photocatalysts for Hydrogen Evolution. *ChemSusChem* **2018**, *11*, 688−699.
(39) Salama, I.; El-Raghy, T.; Barsoum, M. W. Synthesis and Mechanical Properties of Nb_2AlC and $(Ti,Nb)_2AlC$. *J. Alloys Compd.* **2002**, *347*, 271−278.
(40) Cordero, B.; Gómez, V.; Platero-Prats, A. E.; Revés, M.; Echeverría, J.; Cremades, E.; Barragán, F.; Alvarez, S. Covalent Radii Revisited. *Dalton Trans.* **2008**, *21*, 2832−2838.
(41) Hu, C.; Li, F.; Zhang, J.; Wang, J.; Wang, J.; Zhou, Y. Nb_4AlC_3: A New Compound Belonging to the MAX Phases. *Scr. Mater.* **2007**, *57*, 893−896.
(42) Halim, J.; Chartier, P.; Basyuk, T.; Prikhna, T.; Caspi, E. N.; Barsoum, M. W.; Cabioc'h, T. Structure and Thermal Expansion of $(Cr_xV_{1-x})_{n+1}AlC$ n Phases Measured by X-Ray Diffraction. *J. Eur. Ceram. Soc.* **2017**, *37*, 15−21.
(43) Zhou, Y.; Meng, F.; Zhang, J. New MAX-Phase Compounds in the V−Cr−Al−C System. *J. Am. Ceram. Soc.* **2008**, *91*, 1357−1360.
(44) Khazaei, M.; Ranjbar, A.; Esfarjani, K.; Bogdanovski, D.; Dronskowski, R.; Yunoki, S. Insights into Exfoliation Possibility of MAX Phases to MXenes. *Phys. Chem. Chem. Phys.* **2018**, *20*, 8579−8592.
(45) Naguib, M.; Unocic, R. R.; Armstrong, B. L.; Nanda, J. Large-scale Delamination of Multi-layers Transition Metal Carbides and Carbonitrides "MXenes". *Dalton Trans.* **2015**, *44*, 9353−8.
(46) Halim, J.; Kota, S.; Lukatskaya, M. R.; Naguib, M.; Zhao, M. Q.; Moon, E. J.; Pitock, J.; Nanda, J.; May, S. J.; Gogotsi, Y.; Barsoum, M. W. Synthesis and Characterization of 2D Molybdenum Carbide (MXene). *Adv. Funct. Mater.* **2016**, *26*, 3118−3127.
(47) Ashton, M.; Mathew, K.; Hennig, R. G.; Sinnott, S. B. Predicted Surface Composition and Thermodynamic Stability of MXenes in Solution. *J. Phys. Chem. C* **2016**, *120*, 3550−3556.
(48) Anasori, B.; Shi, C.; Moon, E. J.; Xie, Y.; Voigt, C. A.; Kent, P. R.; May, S. J.; Billinge, S. J.; Barsoum, M. W.; Gogotsi, Y. Control of Electronic Properties of 2D Carbides (MXenes) by Manipulating their Transition Metal Layers. *Nanoscale Horizons* **2016**, *1*, 227−234.
(49) Jiang, H.; Johnson, C.; Wang, K. Giant Negative Magneto-resistance of a Degenerate Two-Dimensional Electron Gas in the Variable-range-hopping Regime. *Phys. Rev. B: Condens. Matter Mater. Phys.* **1992**, *46*, 12830.
(50) Zhao, H. L.; Spivak, B. Z.; Gelfand, M. P.; Feng, S. Negative Magnetoresistance in Variable-range-hopping Conduction. *Phys. Rev. B: Condens. Matter Mater. Phys.* **1991**, *44* (19), 10760.
(51) Gu, H.; Guo, J.; He, Q.; Jiang, Y.; Huang, Y.; Haldolaarachige, N.; Luo, Z.; Young, D. P.; Wei, S.; Guo, Z. Magnetoresistive Polyaniline/multi-walled Carbon Nanotube Nanocomposites with Negative Permittivity. *Nanoscale* **2014**, *6*, 181−189.
(52) Sybous, A.; El Kaaouachi, A.; Hemine, J.; Narjis, A.; Limouny, L.; Dlimi, S.; Abdia, R.; Biskupski, G. Negative Magnetoresistance Behaviour and Variable Range Hopping Conduction in Insulating NbSi Amorphous Alloys at Very Low Temperature with Magnetic Field. *J. Mod. Phys.* **2012**, *3*, 521.

DOI: 10.1021/acsanm.8b00332
ACS Appl. Nano Mater. 2018, 1, 2455−2460